Check for updates

Author Manuscript

Low-Temperature Methane Activation Reaction Pathways over Mechanochemically-generated Ce^{4+}/Cu^{+} interfacial sites

Silvia Mauri[§], Rudy Calligaro[§], Carlo Federico Pauletti, Matteo Farnesi Camellone,

Marta Boaro, Luca Braglia, Stefano Fabris, Simone Piccinin[*], Piero Torelli[*], Alessandro Trovarelli*

Dr. S. Mauri, Dr. M. Farnesi Camellone, Dr. L. Braglia, Dr. S. Fabris, Dr. S. Piccinin*, Dr. P. Torelli*
CNR- Istituto Officina dei Materiali
TASC Laboratory, 34149 Trieste, Italy

E-mail: piccinin@iom.cnr.it , piero.torelli@elettra.eu

Dr. R. Calligaro, Professor M. Boaro, Professor A. Trovarelli*
Dipartimento Politecnico and INSTM
Università degli Studi di Udine
Via del Cotonificio 108, 33100 Udine, Italy
E-mail: alessandro.trovarelli@uniud.it

Mr. C. F. Pauletti
Physics Department
Università degli Studi di Trieste
Via Alfonso Valerio 2, 34127 Trieste, Italy

Dr. L. Braglia

AREA Science Park

Padriciano 99, I-34149 Trieste, Italy

Supporting information for this article is given via a link at the end of the document.

This is the author manuscript accepted for publication and has undergone full peer review but has not been through the copyediting, typesetting, pagination and proofreading process, which may lead to differences between this version and the Version of Record. Please cite this article as doi: 10.1002/smll.202403028.

This article is protected by copyright. All rights reserved.

Author Manuscript

Abstract: Methane is a valuable resource and its valorization is an important challenge in heterogeneous catalysis. Here we show that CeO_2/CuO composite prepared by ball milling activates methane at a temperature as low as 250°C. In contrast to conventionally prepared catalyst we also observed the formation of partial oxidation products such as methanol and formaldehyde. Through an *in situ* Diffuse Reflectance Infrared Fourier Transform Spectroscopy (DRIFTS) and *operando* Near Edge X-Ray Absorption Fine Structure Spectroscopy (NEXAFS) approach, we were able to establish that this unusual reactivity can be attributed to the presence of Ce^{4+}/Cu^{+} interfaces generated through a redox exchange between Ce^{3+} and Cu^{2+} atoms facilitated by the mechanical energy supplied during milling. DFT modeling of the electronic properties confirms the existence of a charge transfer mechanism. These results demonstrate the effectiveness and distinctiveness of the mechanical approach in creating unique and resilient interfaces thereby enabling the optimization and refining of CeO_2/CuO catalysts in methane activation reactions.

Introduction

Nowadays, the world has entered in a period of great changes, which boosted the social awareness towards the need of a new paradigm of sustainable and resilient development, which comprehends all the fields of society. A mandatory challenge regards the energetic and environmental field, with the need of development of new materials and technologies for the energy transition, by keeping in mind the fact that these materials must be cheap, abundant and of easy preparation[1]. Catalysis, both homogeneous and heterogeneous, historically played, and plays nowadays, an important role in the field of energy and environmental industrial applications[2]. Specifically, cerium oxide-based catalysts have proven to be excellent materials for applications such as auto exhaust treatment, VOCs abatement and reforming reactions[3]. However, many of these applications use CeO_2 as a support and rely on precious metals as active phase. Cerium oxide (CeO_2) is a well-known material/support because of its excellent redox properties associated with the presence of Ce^{4+}/Ce^{3+} redox couple[4] which can be enhanced by the introduction of transition/noble metals. This enhancement is a result of metal-support interaction[5] which describes the geometrical, electronic and bifunctional modifications occurring at the interfaces of metal and support[6]. The new paradigm in catalysts development requires the use of more sustainable material design[7]. For these reason, Copper-Ceria formulations gained considerable attention through the years for their good catalytic activity in environmental reactions such as the oxidation of Volatile Organic Compounds (VOCs)[8], water gas shift (WGS) reaction[9], and CO preferential Oxidation (CO-PROX)[10]. The favorable characteristics of these systems, combined with the lower cost compared to noble metal-based catalysts, pushed scientific research toward identifying the specific catalytic active sites/interfaces responsible for the good catalytic performance. It is now well-established that the catalytic activity is heavily influenced by copper-ceria interactions thanks to various effects such as (i) the formation of $Cu^{2+}/Cu^{+}/Cu$ and Ce^{4+}/Ce^{3+} redox pairs[5a,11], (ii) the facilitation of the reduction process as compared to single CeO_2 and CuO[12], (iii) the formation of oxygen vacancies[13] and (iv) the stabilization of active intermediates at the interface[5a,14]. The use of inverse catalysts, i.e. oxide particles supported on metal surfaces, combined with the use of the advanced *in situ* and *operando* spectroscopic techniques, has provided important clues in the field[5a,15]. Rodriguez et al. studied an inverse $CeO_2/Cu_xO/Cu(111)$ model catalysts in several reactions such as CO oxidation and water gas shift obtaining better catalytic performances compared to those of a classic Cu/CeO_2 catalysts and to the single components[16]. In addition, the same system was tested in methane oxidation to methanol[17] providing significant evidence supporting a water mediated activation of the C-H bond of methane, which was found to be related to the presence of the Ce^{4+}/Cu^{+} sites/interfaces. Here, we prepared a CeO_2/CuO inverse catalyst by ball milling; the method is easy, clean and scalable, and the mechanical energy provided by the synthesis can be used to modify the interface/active sites at the nanoscale[18]. The milled composite was compared with an equivalent material, synthesized via a procedure

This article is protected by copyright. All rights reserved.

16136829, 2024, 42, Downloaded from https://onlinelibrary.wiley.com/doi/10.1002/smll.202403028 by CNR GROUP II Istituto di Scienza dell', Wiley Online Library on [06/03/2025]. See the Terms and Conditions (https://onlinelibrary.wiley.com/terms-and-conditions) on Wiley Online Library for rules of use; OA articles are governed by the applicable Creative Commons License

in which no mechanical energy was involved. The materials were characterized by means of X Ray Diffraction (XRD), Scanning Electron Microscopy (SEM), Brunauer-Emmett-Teller (BET), Temperature Programmed Reduction (TPR), *in situ* Diffuse Reflectance Infrared Fourier Transform Spectroscopy (DRIFTS) and *operando* Near Edge X-Ray Absorption Fine Structure Spectroscopy (NEXAFS). In particular by coupling *in situ* DRIFTS and *operando* NEXAFS spectroscopies, we have been able to attribute the unusual functionalities of the milled composite to the presence of Ce/Cu interface generated by the mechanical energy provided by the synthesis, that upon heating promotes the redox reaction between Ce^{3+} and Cu^{2+} to give Ce^{4+}/Cu^{+} interface which has been considered responsible for the low temperature (250°C) methane activation also towards partial oxidation products. The electronic and catalytic properties of the composite were modeled using Density Functional Theory (DFT) simulations, providing further evidence for charge transfer occurring between CeO_2 and CuO during interface formation. Furthermore, the calculations predict that the formation energy of oxygen vacancies at the interface is significantly lower compared to that of the two parent oxides. Some of these interfacial sites are also particularly reactive towards the dissociative adsorption of methane. The unusual reactivity found for the ball-milled CeO_2/CuO catalyst at low temperatures, combined with the straightforward and environmentally friendly synthetic procedure, suggests its potential for further study.

Results and Discussion

Ex situ Characterization of CeO_2/CuO Systems

Catalyst	Avg. CuO Particle Size (nm)	Avg. CeO_2 Particle Size (nm)	BET Surf. Area (m^2/g)	Avg. Pore Diameter (Å)	Mean Pore Volume (cm^2/g)

This article is protected by copyright. All rights reserved.

Author Manuscript

WILEY VCH

16136829, 2024, 42, Downloaded from https://onlinelibrary.wiley.com/doi/10.1002/smll.202403028 by CNR GROUP II Istituto di Scienza dell', Wiley Online Library on [06/03/2025]. See the Terms and Conditions (https://onlinelibrary.wiley.com/terms-and-conditions) on Wiley Online Library for rules of use; OA articles are governed by the applicable Creative Commons License

Figure 1 summarizes the morphological and textural characteristics of the two samples. One sample was prepared by conventional impregnation (I-CeO_2/CuO), while the other was produced through ball milling (M-CeO_2/CuO). Schematic representations of the two methods are reported in **Figure 1a** and **Figure 1b** respectively. BET adsorption isotherm plots of the two composites is reported in **Figure 1f**, showing that the impregnated sample has larger pores when compared with the milled one (see also **Table 1** and **Figure S1**). The latter has the same pore distribution of the pristine mesoporous CeO_2[19], while CuO does not show the presence of a similar micro/mesoporous structure (**Table 1 and Figure S1**).

Table 1. Summary of results obtained from XRD and BET analysis.

CuO	19.5	-	10	351	0.09
CeO_2	-	8.7	115	72	0.30
M-CeO_2/CuO	19.9	8.6	30	180	0.18
I-CeO_2/CuO	19.5	6.1	20	266	0.15

It is evident from Scanning Electron Microscopy (**Figure 1c** and **Figure 1d)** that both materials have similar morphologies, since both consist of large CeO_2 aggregates (about 3 μm in size) made up of small crystallites (see **Table 1**) covered by CuO particles. **Figure S2** shows SEM images of the two samples where a more uniform surface coverage is observed resulting in a higher degree of homogeneity in the I-CeO_2/CuO composite compared to the M-CeO_2/CuO sample. The different contrast obtained using a backscattered electrons analyzer and an energy dispersive X-Ray spectroscopy analysis performed on three different sample regions (shown in **Figures S3-S4**) allowed to assign the first species to CeO_2 and the second to CuO, as can be observed in the table of **Figure S3**. The X-ray diffraction patterns of the two composites (**Figure 1e**) show the characteristic peaks of fluorite CeO_2 and monoclinic CuO[20].

Author Manuscript

This article is protected by copyright. All rights reserved.

16136829, 2024, 42, Downloaded from https://onlinelibrary.wiley.com/doi/10.1002/smll.202403028 by CNR GROUP II Istituto di Scienza dell', Wiley Online Library on [06/03/2025]. See the Terms and Conditions (https://onlinelibrary.wiley.com/terms-and-conditions) on Wiley Online Library for rules of use; OA articles are governed by the applicable Creative Commons License

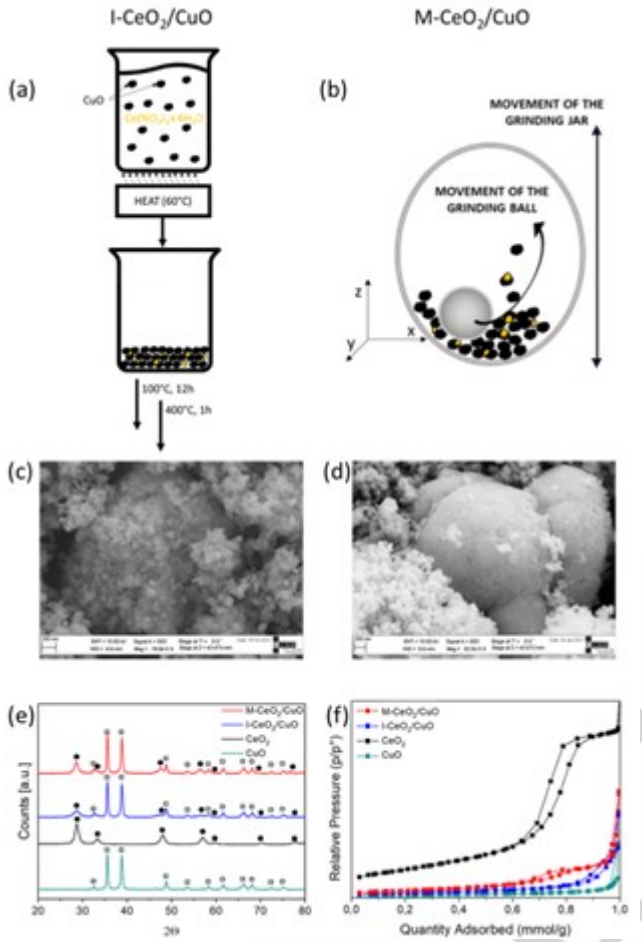

Figure 1. (a) Schematic representation of the synthetic procedure adopted for the I-CeO_2/CuO composite. (b) Schematic representation of the synthetic procedure adopted for the M-CeO_2/CuO composite. (c) Scanning Electron Microscopy image of I-CeO2/CuO composite. (d) Scanning Electron Microscopy image of M-CeO_2/CuO composite. (e) X-Ray Diffraction patterns of M-CeO_2/CuO, I-CeO_2/CuO, and pristine CeO_2 and CuO. (f) Adsorption isotherm plots of M-CeO_2/CuO, I-CeO_2/CuO, and pristine CeO_2 and CuO.

The I-CeO_2/CuO shows broader CeO_2 peaks compared to the milled counterpart. This difference indicates that smaller CeO_2 crystallites are present, as evidenced by Sherrer's analysis (see **Table 1**), and could be related to the different calcination temperature of the CeO_2 phase in the two samples (see Methods section in the Supplementary Information). A similar behaviour characterizes the reducibility of the two samples monitored by Temperature Programmed Reduction (TPR) analysis, with a shift to lower temperatures of the CuO (≃20°C) and bulk CeO_2 (≃100°C) reduction peaks, that are symptomatic of the interaction between CuO and CeO_2[20,21] (see **Figure S5**).

Ball Milling Process and Thermal Activation of CeO_2/CuO systems

The experimental procedure followed for the *in situ* DRIFT and *operando* NEXAFS characterization is schematically reported in **Scheme 1** and described in detail in **Section S2** and **Figure S6**.

This article is protected by copyright. All rights reserved.

Author Manuscript

16136829, 2024, 42, Downloaded from https://onlinelibrary.wiley.com/doi/10.1002/smll.202403028 by CNR GROUP II Istituto di Scienza dell', Wiley Online Library on [06/03/2025]. See the Terms and Conditions (https://onlinelibrary.wiley.com/terms-and-conditions) on Wiley Online Library for rules of use; OA articles are governed by the applicable Creative Commons License

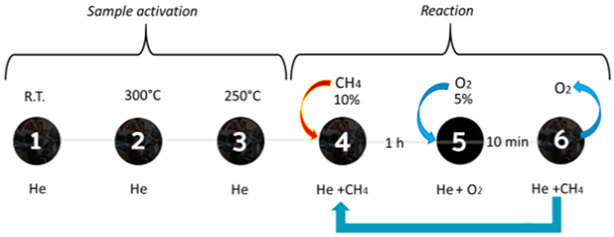

Scheme 1. Scheme of the experimental procedure employed for the *in situ* DRIFTS and *operando* NEXAFS experiments. All the steps have been performed at 1 bar of total pressure.

The experimental protocol consists of three initial steps related to the thermal activation of the catalyst, whose results are described below, and three subsequent steps related to its interaction with CH_4 and O_2, in a manner similar to that reported in previous studies[15], which are described in the next section. **Figure 2** show an enlarged view of the Cu L_3 and the Ce M_5 edge NEXAFS spectra of the I-CeO_2/CuO (**Figure 2a-2b**) and the M-CeO_2/CuO (**Figure 2e-2f**) samples acquired during steps 1 and 3 of the experimental procedure, together with the spectra of the precursors used for the ball milling synthesis (i.e. CuO and CeO_2, **Figure 2c-2d** respectively). The complete Cu $L_{2,3}$ and Ce $M_{4,5}$, together with O K edge spectra with detailed description are shown in **Figure S7-S8** of **Section S3**. The structures at 931.05 eV and 939.0 eV, detected in all the Cu L_3 edge spectra of **Figure 2**, are characteristic of the $2p_{3/2} \rightarrow 3d$ and $2p_{3/2} \rightarrow 4s$ electronic core excitation of Cu^{2+} atoms[22]. At room temperature, no other features are present. Regarding the Ce M_5 edge spectra, the I-CeO_2/CuO material (**Figure 2b**) shows the characteristic features of CeO_2 located at 882.5 and 887.8 eV, with Ce atoms

This article is protected by copyright. All rights reserved.

Author Manuscript
WILEY VCH
16136829, 2024, 42, Downloaded from https://onlinelibrary.wiley.com/doi/10.1002/smll.202403028 by CNR GROUP II Istituto di Scienza dell', Wiley Online Library on [06/03/2025]. See the Terms and Conditions (https://onlinelibrary.wiley.com/terms-and-conditions) on Wiley Online Library for rules of use; OA articles are governed by the applicable Creative Commons License

having a

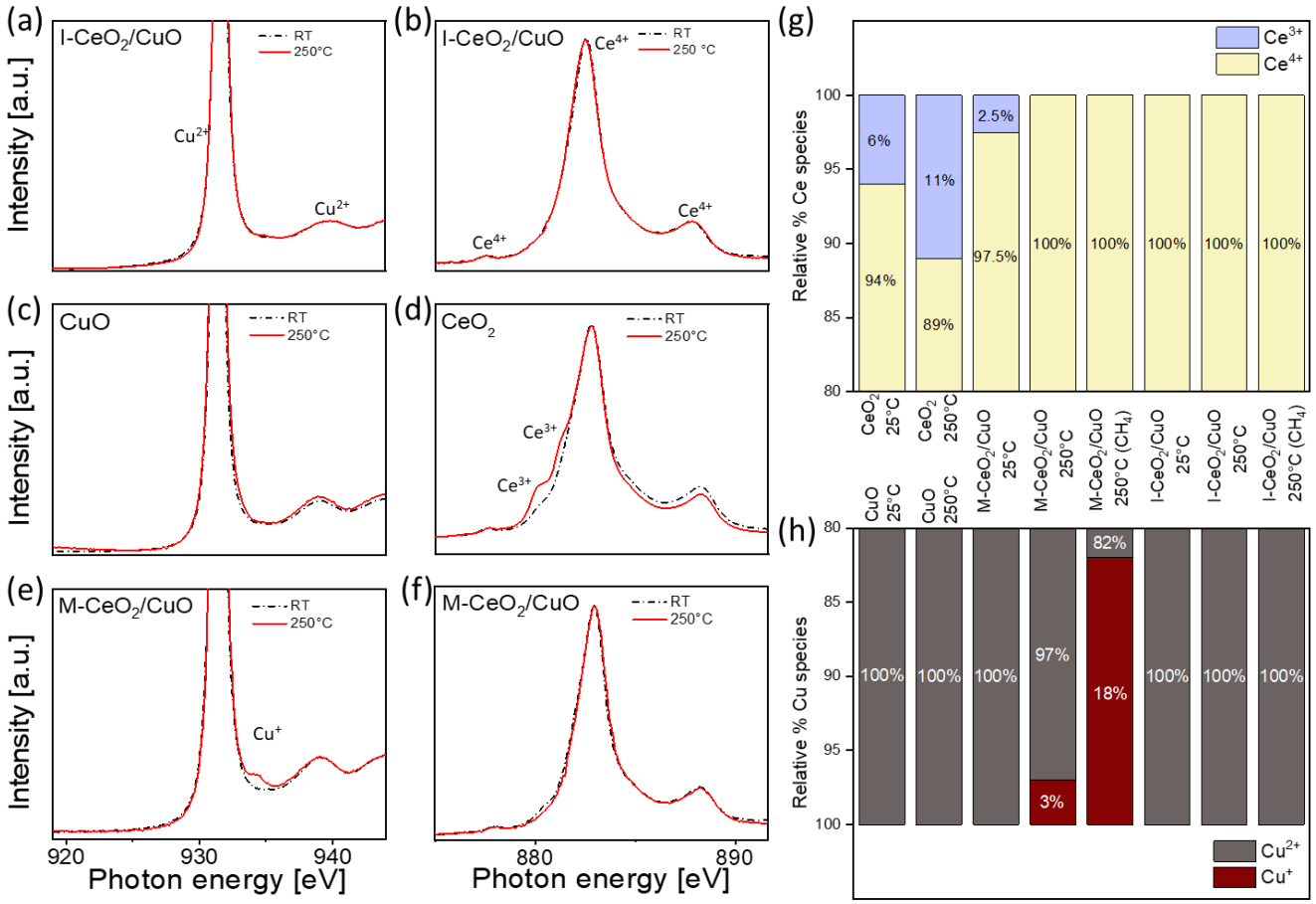

Figure 2. (a),(c),(e) Cu L_3 edge NEXAFS spectra of I-CeO_2/CuO, CuO nanoparticles used as precursors and M-CeO_2/CuO respectively. (b),(d),(f) Ce M_5 edge NEXAFS spectra of I-CeO_2/CuO, the CeO_2 used as precursor for the milled composite and M-CeO_2/CuO respectively. Dotted black lines: spectra acquired at room temperature; red lines: spectra acquired at 250°C after the thermal activation to 300°C. (g) Ce^{4+}/Ce^{3+} concentrations under different treatment conditions. (h) Cu2+ and Cu^{+} concentrations under different treatment conditions.

+4 oxidation state. Another weak structure located at 877.4 eV is observed, according to literature related to Ce^{4+}, yet with an uncertain attribution[23]. In the room temperature spectrum of the CeO_2 used for the preparation of the milled composite (**Figure 2d**), in addition to the Ce^{4+} peaks, two shoulders appear at lower photon energies with respect to the main Ce^{4+} structure, at 880.4 eV and 881.5 eV. These shoulders are attributable to Ce^{3+} [24] and are consistent with the expected high concentration of surface Ce^{3+} atoms of the high surface area ceria used. Through a linear combination fitting procedure (see **Supplementary Section 4** for details) we estimated the relative concentration of Ce^{3+} in pristine CeO_2 to be around 6% (**Figure S9** and **Figure 2g**). The same shoulders are present in the M-CeO_2/CuO spectrum with a lower intensity (2.5% according to the linear combination fit, **Figure 2g**), indicating a substantial Ce^{3+} oxidation during the milling process with CuO. After the heating ramp, cleaning and dehydration of the surface occurs[25] (see **Figure S8**), revealing the formation of Cu^{+} sites, along with the oxidation of the corresponding amount of Ce^{3+} (**Figure 2g-2h**), which does not occur on the I-CeO_2/CuO material. This demonstrates the effectiveness of the ball milling treatment in creating

This article is protected by copyright. All rights reserved.

Author Manuscript

16136829, 2024, 42, Downloaded from https://onlinelibrary.wiley.com/doi/10.1002/smll.202403028 by CNR GROUP II Istituto di Scienza dell', Wiley Online Library on [06/03/2025]. See the Terms and Conditions (https://onlinelibrary.wiley.com/terms-and-conditions) on Wiley Online Library for rules of use; OA articles are governed by the applicable Creative Commons License

Author Manuscript

the optimal configuration of the Ce^{3+}/Cu^{2+} interface which upon heating facilitates redox exchange resulting in the formation of Ce^{4+} and Cu^{+}. At 250°C, the relative concentrations of Ce^{3+} and Cu^{+} in the M-CeO_2/CuO are 0% and 3%, respectively, while the pristine oxides analyzed at the same temperature show a concentration of 11% and 0% (**Figure 2g-2h**).

The tendency of the electronic charge to migrate from CeO_2 to CuO upon interfacing has been validated with DFT calculations. Two different models have been constructed to represent the CeO_2/CuO composite (see **Section S5** for further details): one that exposes the CeO_2(110) and CuO(101) surface terminations, and one that exposes the CeO_2(111) and CuO(-111) surface terminations; these are among the most stable surfaces for the two isolated oxides (see **Figure S11**). **Figure 3b** shows the charge migration from the CeO_2(110) side to the CuO(101) side of the stoichiometric composite, with its top view depicted in **Figure 3a**. Bader charge analysis indicates that a total of 0.64*e* migrate from CeO_2 to CuO. Charge depletion on the CeO_2 side of the composite is mainly localized in proximity of the interface whereas charge accumulation on the CuO portion is completely delocalized. A larger charge transfer occurs when a defective CeO_2(110) slab (i.e. containing one oxygen vacancy, representative for the defective CeO_2 used in the milled composite) and a stoichiometric CuO(101) slab are merged (**Figures 3c-3d**), with a total of 1.20*e* migrating from CeO_2 to CuO.

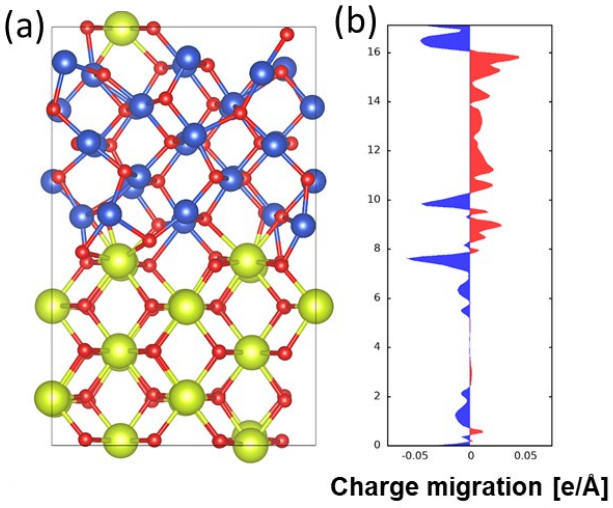

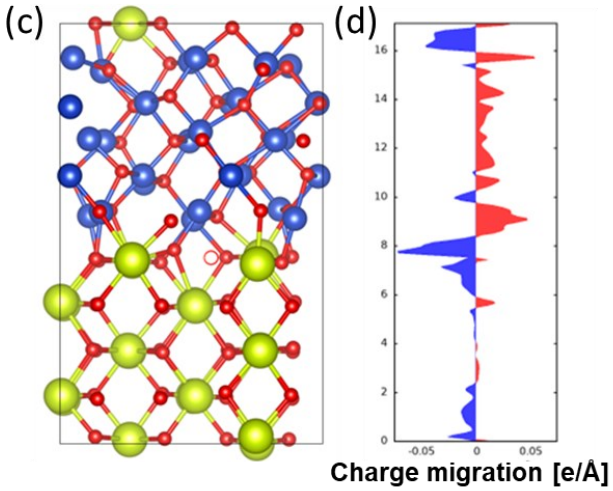

This article is protected by copyright. All rights reserved.

16136829, 2024, 42, Downloaded from https://onlinelibrary.wiley.com/doi/10.1002/smll.202403028 by CNR GROUP II Istituto di Scienza dell', Wiley Online Library on [06/03/2025]. See the Terms and Conditions (https://onlinelibrary.wiley.com/terms-and-conditions) on Wiley Online Library for rules of use; OA articles are governed by the applicable Creative Commons License

Figure 3. (a),(c) Models of the respectively stoichiometric and defective CeO_2(110) CuO(101) clusters employed for the DFT calculations; red balls: Oxygen, yellowish balls: Cerium, blue balls: Copper. (b), (d) Calculated charge transfer for respectively stoichiometric and defective CeO_2(110) to CuO(101) surfaces consequent to their merging.

In support of this argument, the occupations of Ce-4f orbitals in an isolated CeO_2(110) slab with an oxygen vacancy reveal the presence of two Ce^{3+} ions, while in the composite only one Ce^{3+} ion remains: this clearly indicates that one of the two electrons has a strong tendency to migrate towards the CuO side. We found similar results for the CeO_2(111)/CuO(-111) interface, with Bader charge analysis showing a total of 0.95*e* migrating from CeO_2 towards CuO upon interfacing stoichiometric compounds and 1.69*e* in the presence of an oxygen vacancy in CeO_2. Furthermore, creating oxygen vacancies at the interface costs significantly less if compared to the two parent oxides. The lowest oxygen vacancy formation energies (E_{vac}) calculated in the CeO_2(111)/CuO(-111) and CeO_2(110)/CuO(101) interfaces are -0.17 eV and 0.17 eV respectively. These values are considerably lower compared to similar sites in the pristine surface terminations of the two isolated oxides, as seen from **Table S1**. Indeed, based on ab initio thermodynamics, we predict the presence of oxygen vacancies in both models of the interface within the range of temperatures and oxygen partial pressures utilized in the experiments (see **Figure S13**). The experimental and theoretical results obtained confirm the key role played by the defective surface Ce^{3+} sites in influencing the interfacial redox process. The different behaviour between the M-CeO_2/CuO and the I-CeO_2/CuO suggests that in the latter the interfacial charge redistribution resulting from the oxides merging is more delocalised and not sufficient to reduce Cu^{2+} atoms to Cu^{+}, probably due a lower concentration of Ce^{3+}. It is also plausible that the thermal treatment applied on the impregnated sample suppresses the generation of oxygen vacancies, as suggested by other researchers[8]. On the other hand, the mechanical action provided in the synthesis of M-CeO_2/CuO may play a key role in the enhancement of the interfacial charge transfer phenomena.

Methane activation and oxidation in CeO_2/CuO systems

After the thermal activation, we studied the interaction between the composites and the gas reactants (CH_4 and O_2) by combining *operando* NEXAFS and *in situ* DRIFT spectroscopies. We closely monitored the evolution of the catalyst surface electronic structure and the formation of adsorbates during the catalytic reaction. **Figure S12** depicts a 3D rendering of the *operando* NEXAFS reaction cell developed at the APE-HE beamline[26].

This experimental set up allows to perform NEXAFS analysis in the soft x ray range at 1 bar, thereby filling the so-called "pressure gap"[27] which has long affected the soft x rays due to their low penetration. The reaction cell allows the continuous acquisition of the spectra at 1 bar of total pressure, under real catalytic conditions[28]. Meanwhile the reaction products are detected by an online micro-GC (details are provided in the Methods section of the Supporting Information and in **Section S6 (Figure S13, S14)**. **Figures 4a-4b** illustrate the Cu L_3 edge NEXAFS spectral evolution (from the bottom to the top) of the two composites during their exposure to a CH_4(10%)/He(90%) mixture for 1 hour at 250°C. Consistent spectral modifications are detected in the M-CeO_2/CuO composite: the Cu^{+} related structure increases in intensity and reaches a maximum after 30 minutes of methane exposure. The linear combination fitting analysis reveals that at this stage the relative concentration of Cu^{+} is 18% (**Figure 2h** and **S10**). It then becomes broader and decreases in intensity reaching a stationary shape after 60 minutes.

This article is protected by copyright. All rights reserved.

Author Manuscript

16136829, 2024, 42, Downloaded from https://onlinelibrary.wiley.com/doi/10.1002/smll.202403028 by CNR GROUP II Istituto di Scienza dell', Wiley Online Library on [06/03/2025]. See the Terms and Conditions (https://onlinelibrary.wiley.com/terms-and-conditions) on Wiley Online Library for rules of use; OA articles are governed by the applicable Creative Commons License

Author Manuscript

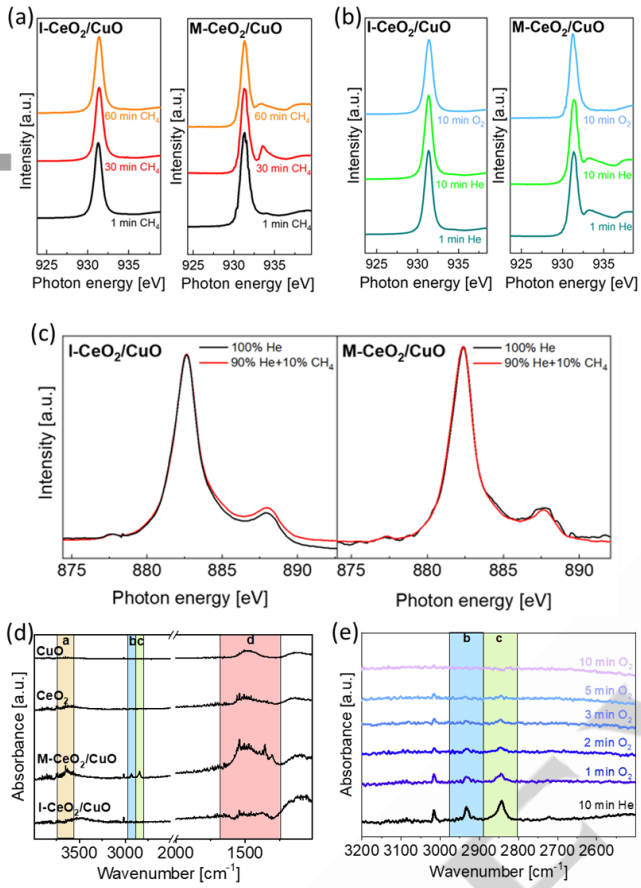

Figure 4. (a) Cu L_3 edges NEXAFS spectra evolution of I-CeO_2/CuO and M-CeO_2/CuO acquired during the exposure to a CH_4(10%)/He(90%) mixture for 1 hour, at 250°C and at 1 bar of total pressure. (b) Cu L_3 edges NEXAFS spectra evolution of I-CeO_2/CuO and M-CeO_2/CuO acquired in He(100%) atmosphere, after the exposure to a CH_4(10%)/He(90%) mixture for 1 hour, and introducing a He(95%)/O_2(5%) mixture for 10 minutes. (c) Ce M_5 edge NEXAFS spectra of I-CeO_2/CuO and M-CeO_2/CuO acquired in He(100%) atmosphere (black lines), and during the exposure to a CH_4(10%)/He(90%) mixture for 1 hour (red lines). (d) DRIFT spectra acquired in He(100%) atmosphere at 250°C and at 1 bar, after exposing CuO, CeO_2, M-CeO_2/CuO and I-CeO_2/CuO samples to a CH_4(10%)/He(90%) mixture for 1 hour. (e) DRIFT spectra evolution of M-CeO_2/CuO acquired in He(95%)/O_2(5%) atmosphere at 250°C and at 1 bar.

These results indicate that CH_4 perturbs the chemical environment of Cu atoms resulting in a significant reduction of active sites. The position of the Cu^+ peak (933.15 eV) is slightly shifted to lower photon energy in comparison to the Cu_2O white line (933.6 eV), since in the M-CeO_2/CuO composite Cu sites have a different coordination environment with respect to the cuprite structure[25] (**Figure S15** shows the comparison between Cu^+ features of M-CeO_2/CuO composite and reference spectra of CuO and Cu_2O powders). Conversely, the I-CeO_2/CuO spectra clearly show that the electronic structure is unchanged upon CH_4 exposure to methane. After removing CH_4 from the reaction mixture (dark and light green spectra in **Figure 4b**), the structure related to reduced Cu sites persists in the NEXAFS spectra of the M-CeO_2/CuO composite, maintaining both the shape and intensity. This indicates that the activated CH_4 is chemisorbed on the catalyst surface, resulting in an irreversible perturbation of the local chemical environment of a portion of the Cu surface sites. At the same time, the Ce $M_{4,5}$ edge spectra do not change in both catalysts (**Figure 4c**), maintaining the characteristic

This article is protected by copyright. All rights reserved.

16136829, 2024, 42, Downloaded from https://onlinelibrary.wiley.com/doi/10.1002/smll.202403028 by CNR GROUP II Istituto di Scienza dell', Wiley Online Library on [06/03/2025]. See the Terms and Conditions (https://onlinelibrary.wiley.com/terms-and-conditions) on Wiley Online Library for rules of use; OA articles are governed by the applicable Creative Commons License

features of CeO_2. To further elucidate how methane activates on the M-CeO_2/CuO catalyst surface, DRIFT spectra were acquired during and after exposure to CH_4 (See extended spectra in **Figure S16** of **Section S7**). The experiment was replicated for the I-CeO_2/CuO composite and for the single oxides. The results are illustrated in **Figure 4d** with extended spectra in **Figure S16**. Focusing on the spectrum of the M-CeO_2/CuO composite, we observe the presence of several bands after the exposure to CH_4, which have been assigned to partially oxidized methane intermediates of general formula $C_xH_yO_Z$ which includes formates, methoxy and hydrogen carbonates[29] (streching modes indicated as ***b*** and ***c*** in Figure 4d-4e and related bending modes indicated as ***d*** in Figure 4d (see also **Table S2** for details). These intermediates are likely formed as a consequence of CH_4 deprotonation. No activation was observed in the pristine CuO and CeO_2, as well as in the impregnated analogue of the ball milled sample (See Figure **S18** for a clearer comparison between M-CeO_2/CuO and I-CeO_2/CuO). This indicates that oxygen atoms of the composite are responsible for the CH_4 deprotonation. The growth of structure in the O-H stretching region indicated as ***a*** in Figure 4d supports this inference[29c,30]. Combining the information obtained from the NEXAFS and DRIFT spectra we hypothesized that the reactive O atoms are located close to specific CuO-CeO_2 interfaces formed during the ball milling process. The formation of -OH species as a consequence of CH_4 deprotonation, observed in DRIFT spectra, is likely to occur at the interface between CeO_2 and CuO, and can be then responsible for the Cu reduction observed in NEXAFS spectra (**Figure 4a**). This hypothesis is supported by DFT calculations, which show how dissociative methane adsorption is thermodynamically favored on atoms near the CeO_2(111)/CuO(-111) and CeO_2(110)/CuO(-110) interfaces, as evidenced in **Section S8** (**Table S3)**. The dissociative methane adsorption energy at the most favorable sites of the two interfaces is significantly more exothermic than that of any of the isolated parent surfaces, with values of -3.28 and -2.19 eV for the two stoichiometric interfaces. Indeed, these values are at least 0.7 eV and up to 1 eV more exothermic than similar sites on the same surface terminations of the two parent oxides (**Table S3**). In the presence of an oxygen vacancy, the value increases to -2.40 eV at the first interface. The value remains more favourable compared with the results obtained for the parent oxides. On the other hand, with the second model, the adsorption energy is -1.76 eV, which is close with what found on the parent oxides. Consequently, the impact of the presence of oxygen vacancies on the adsorption of methane differs between the two models, and is therefore influenced by the structural details of the interface. Moreover, on the CeO_2(111)/CuO(-111) interface we identified a number of surface sites which exhibit similar chemical environments (i.e. bond distances and atomic charges) but remarkably different methane adsorption energies (**Figure S22**). As shown in **Section S11** however, no clear correlation can be observed between the methane adsorption energy and geometric or electronic structure descriptors of the adsorption sites. Similarly, the activation energy for methane dissociation is highly dependent on the specific structural features of the catalyst surface. There are cases where the influence of the interface is favourable, leading to a significant decrease in the barrier, from 0.98 to 0.57 eV in the case of the stoichiometric CeO_2(111)/CuO(-111) model (**Figure 5f**), and cases that do not show the same effect (such as the CeO_2(110)/CuO(-110) or where oxygen vacancies are present). Thus, the impact of the presence of oxygen vacancies on the adsorption of methane and its activation energy is influenced by the structural details of the interface. Here we have evaluated two specific models, but we need to keep in mind the wide variety of interfaces that are likely to be present in the ball-milled sample, suggesting that the activation of methane could be restricted to a subset of these interfaces. After the 5%O_2/He mixture is introduced in the reaction cell the NEXAFS spectra of the M-CeO_2/CuO composite (**Figure 4b and 5a**), show a disappearance of the structure associated to Cu^+, indicating the re-oxidization of reduced Cu sites to the initial Cu^{2+} electronic configuration. This suggests that O_2 plays a pivotal role in the desorption of the activated CH_4 species, thus restoring the initial electronic configuration of the catalyst surface. The DRIFT spectra of **Figure 4e** (extended spectra reported in **Figure S17**) confirm that the adsorbates are desorbed from the M-CeO_2/CuO catalyst surface upon O_2 exposure, as the peaks related to adsorbed species disappear already after 10 minutes, restoring a clean catalyst surface. The Ce M_5 edge spectrum does not change after oxidation,

This article is protected by copyright. All rights reserved.

Author Manuscript

16136829, 2024, 42, Downloaded from https://onlinelibrary.wiley.com/doi/10.1002/smll.202403028 by CNR GROUP II Istituto di Scienza dell', Wiley Online Library on [06/03/2025]. See the Terms and Conditions (https://onlinelibrary.wiley.com/terms-and-conditions) on Wiley Online Library for rules of use; OA articles are governed by the applicable Creative Commons License

Author Manuscript

as shown in **Figure S19**, indicating that Ce sites maintain a +4 oxidation state throughout all reaction steps. **Figures 5a-5c,** from the bottom to the top, summarize the results obtained during the complete *operando* NEXAFS/*in situ* DRIFT experiment performed on the M-CeO_2/CuO catalyst at 250°C. In order to verify the occurrence of the surface reaction and to identify the different reaction products, we monitored the *operando* NEXAFS reaction cell gas output through an online Micro-GC. The results are reported in **Figure 5c**, where the CH_2O and CH_3OH regions are shown (for the complete chromatograms refer to **Figure S20-S21)**.

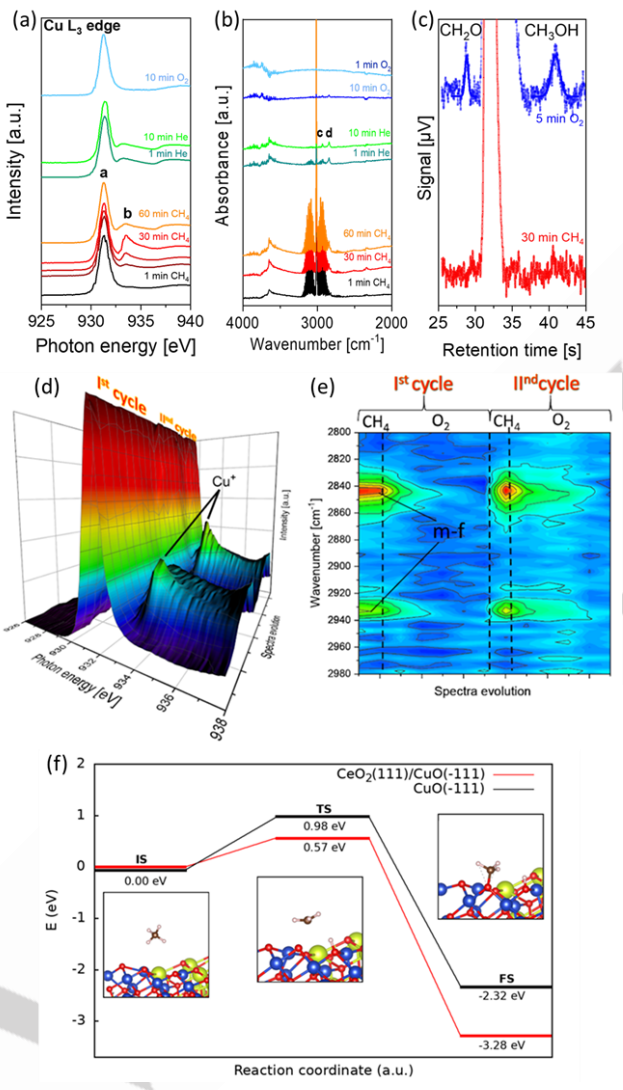

Figure 5. (a) Cu L_3 NEXAFS, (b) DRIFT, (c) Micro-GC spectra evolution during the different reaction steps. Black and red-based lines: spectra acquired exposing the M-CeO_2/CuO catalyst to the He(90%)/CH_4(10%) reaction mixture; green-based lines: spectra acquired exposing the catalyst to the He(100%) reaction mixture; Blue-based lines: spectra acquired exposing the catalyst to the He(95%)/O_2(5%) reaction mixture. (d) Cu L_3 edge NEXAFS and (e) DRIFT spectra acquired during two subsequent He → CH_4/He → O_2/He catalytic cycles, showing how the electronic structure of Cu is totally recovered at the end of every cycle, in conjunction with the adsorption (in CH_4) and desorption (in O_2) of methoxy and formate species (m-f) on the catalyst surface. (f) Reaction path of dissociative methane adsorption. Energies of initial, transition and final states along the path for

This article is protected by copyright. All rights reserved.

16136829, 2024, 42, Downloaded from https://onlinelibrary.wiley.com/doi/10.1002/smll.202403028 by CNR GROUP II Istituto di Scienza dell', Wiley Online Library on [06/03/2025]. See the Terms and Conditions (https://onlinelibrary.wiley.com/terms-and-conditions) on Wiley Online Library for rules of use; OA articles are governed by the applicable Creative Commons License

dissociative methane adsorption on the CeO_2(111)/CuO(-111) interface (red curve) and on a pristine surface of CuO(-111) (black curve). The insets show the corresponding geometries for the CeO_2(111)/CuO(-111) interface.

In addition to the signals of CH_4 and O_2, that overlap at ≃ 24 s, we detected CO_2 (≃ 25 s) and H_2O (≃ 32 s) upon exposure of the catalyst to CH_4; the two signals increase consistently when the reaction mixture is switched to an oxidizing atmosphere. The presence of minor quantities of CO_2 and H_2O during the exposure to 10%CH_4/He atmosphere could be justified by the total deprotonation of CH_4 in the reactive sites of the milled composite and to the presence of more mobile and reactive oxygens, as confirmed by the DFT calculations. When oxygen is introduced into the reaction cell, $Cu^+ \rightarrow Cu^{2+}$ oxidation is detected by NEXAFS (**Figure 5a, 4b**) together with a gradual disappearance of the signals related to the adsorbed species, indicating desorption of products (**Figure 5b, 4e**). The chromatographic analysis revealed an increase in the total oxidation products (CO_2 and H_2O), together with the appearance of peaks at 28.7 s and 41 s related to the partial oxidation products formaldehyde and methanol, respectively, which were not observed in the I-CeO_2/CuO sample (See **Figure S21**). Moreover, the continuous monitoring of the Cu NEXAFS spectra during the reaction (**Figure 5a**), revealed that after the exposure to He(95%)/O_2(5%) mixture the electronic structure of Cu atoms is fully recovered, as methoxy, formates and carbonates are desorbed from the catalyst surface (**Figure 5b**). Similar results are obtained by repeating steps 4-5-6 as shown in **Figure 5d** (NEXAFS) and **Figure 5e** (DRIFT). This cyclability can be considered as symptomatic of a stable behavior of the material. Overall the results indicate that, the use of mechanical forces to shape metal/support interfaces and organize contact points at a nanoscale level, may lead to unexpected functionalities and promote activation of methane to oxygenates compared to materials prepared by conventional methods.

Conclusion

This study investigated the surface behaviour towards methane activation of a CeO_2/CuO composite synthesized through a green and scalable ball milling technique. A similar CeO_2/CuO material synthesized with a conventional impregnation method was also analyzed for comparison. The standard *ex situ* characterization techniques used to investigate the main features of the material (XRD, TPR, BET and SEM) revealed comparable morphological and structural/reduction properties between the two composites. However, the combined *operando* NEXAFS and *in situ* DRIFT investigation, probed a considerably distinct surface reactivity for the two composites under actual operating conditions. At a temperature of 250°C, the impregnated catalyst was unable to activate methane, resulting inactive for partial oxidation. Conversely, the ball milled composite showed methane activation capabilities. The origin of this behavior was elucidated by NEXAFS spectroscopy combined with DFT calculations, which indicated a net charge transfer occurring from CeO_2 to CuO surfaces following the ball milling process and the thermal activation. The material exhibits specific reactive interfaces which are absent in the conventional impregnated catalyst and whose formation is likely to be favoured by the mechanical energy supplied during milling. The high concentration of Ce^{3+} ions (provided by the use of a high surface area CeO_2 as a precursor for the milled composite), aided by the mechanical action provided by milling, effectively enhancing the Ce → Cu charge transfer, as also demonstrated by DFT calculations. The *In situ* DRIFT investigation showed that methane is adsorbed on the catalyst surface on reactive oxygen atoms, in the form of methane oxidation intermediates $C_xH_yO_z$, which led to the formation of CO_2, H_2O, CH_2O and CH_3OH, detected by the micro-GC directly connected to the *operando* NEXAFS reaction cell during the exposure of the sample to an oxidizing atmosphere. The desorption of products promoted by O_2 restores the initial electronic configuration of the catalyst surface, allowing more cycles to be carried out without deactivation. The in-depth spectroscopic investigation under real catalytic conditions coupled with DFT calculations has demonstrated to be fundamental in identifying the reaction active sites and in describing the reaction mechanism. These were oxygen atoms located close to the CeO_2/CuO interface, able to deprotonate the CH_4, which is consequently

This article is protected by copyright. All rights reserved.

Author Manuscript

16136829, 2024, 42, Downloaded from https://onlinelibrary.wiley.com/doi/10.1002/smll.202403028 by CNR GROUP II Istituto di Scienza dell', Wiley Online Library on [06/03/2025]. See the Terms and Conditions (https://onlinelibrary.wiley.com/terms-and-conditions) on Wiley Online Library for rules of use; OA articles are governed by the applicable Creative Commons License

adsorbed on another O atom of the interface. The oxidizing agent (O_2) acts as a promoter for the products desorption, refilling the created oxygen vacancies and thus recovering the initial catalyst surface. These results could help to pave the way to the design of more robust catalytic systems prepared by sustainable mechanical routes and highlight the role of mechanical activation of interfaces offering a valuable tool for catalyst engineering.

Supporting Information

The authors have cited additional references within the Supporting Information. In Section S1 references have been added to comment TPR profiles reported in figure S5 [31]. Additional references have been added to support the DRIFTS peaks assignation in Table S2 of Section S7 [32]. Two additional references[33] have been added in Section S8 and S9, respectively. Additional references were added also in the experimental Section S13[34].

Acknowledgements

This work has been performed in the framework of the Nanoscience Foundry and Fine Analysis (NFFA-MUR Italy Progetti Internazionali) facility (https://www.trieste.nffa.eu/). L.B. acknowledges the (PNR) grant J95F21002830001 with title "FAIR-by-Design".

Keywords: Mechanochemistry • Operando • Methane • Spectroscopy • Heterogeneous catalysis

[1] a) D. Wang, D. Astruc, *Chem. Soc. Rev.* **2017**, *46*, 816–854. b) M. B. Gawande, A. Goswami, F. X. Felpin, T. Asefa, X. Huang, R. Silva, X. Zou, R. Zboril, R. S. Varma, *Chem. Rev.* **2016**, *116*, 3722–3811.

[2] a) I. Fechete, Y. Wang, J. C. Védrine, *Catal. Today* **2012**, *189*, 2–27. b) A. Trovarelli, C. De Leitenburg, M. Boaro, G. Dolcetti, *Catal. Today* **1999**, *50*, 353–367.

[3] a) T. Wu, R. T. Guo, C. F. Li, W. G. Pan, *J. Environ. Chem. Eng.* **2023**, *11*, 109136. b) M. Boaro, S. Colussi, A. Trovarelli, *Front. Chem.* **2019**, *7*, 28.

[4] a) A. Trovarelli in *Catalysis by Ceria and Related Materials*, Imperial College Press, London, **2002**. b) T. Montini, M. Melchionna, M. Monai, P. Fornasiero, *Chem. Rev.* **2016**, *116*, 5987–6041.

[5] a) S. J. Tauster, S. C. Fung, R. L. Garten, *J. Am. Chem. Soc.* **1978**, *100*, 170–175. b) C. T. Campbell, *Nat. Chem.* **2012**, *4*, 597–598. c) M. Konsolakis, *Appl. Catal. B Environ.* **2016**, *198*, 49–66.

[6] a) L. Kang, B. Wang, A. T. Güntner, S. Xu, X. Wan, Y. Liu, S. Marlow, Y. Ren, D. Gianolio, C. C. Tang, V. Murzin, H. Asakura, Q. He, S. Guan, J. J. Velasco-Vélez, S. E. Pratsinis, Y. Guo, F. R. Wang, *Angew. Chemie - Int. Ed.* **2021**, *60*, 14420–14428. b) M. Cargnello, V. V. T. Doan-Nguyen, T. R. Gordon, R. E. Diaz, E. A. Stach, R. J. Gorte, P. Fornasiero, C. B. Murray, *Science* **2013**, *341*, 771–773.

[7] a) H. Xin, T. Mou, H. S. Pillai, S.-H. Wang, Y. Huang, *Accounts Mater. Res.* **2024**, *5*, 22–34. b) F. Zaera, *Catal. Letters* **2012**, *142*, 501–516.

[8] J. Yun, L. Wu, Q. Hao, Z. Teng, X. Gao, B. Dou, F. Bin, *J. Environ. Chem. Eng.* **2022**, *10*, 107847.

This article is protected by copyright. All rights reserved.

Author Manuscript

16136829, 2024, 42, Downloaded from https://onlinelibrary.wiley.com/doi/10.1002/smll.202403028 by CNR GROUP II Istituto di Scienza dell', Wiley Online Library on [06/03/2025]. See the Terms and Conditions (https://onlinelibrary.wiley.com/terms-and-conditions) on Wiley Online Library for rules of use; OA articles are governed by the applicable Creative Commons License

[9] L. Ilieva, I. Ivanov, P. Petrova, G. Munteanu, Y. Karakirova, J. W. Sobczak, W. Lisowski, E. M. Anghel, Z. Kaszkur, T. Tabakova, *Int. J. Hydrogen Energy* **2020**, *45*, 26286–26299.

[10] C. G. M. Reis, K. A. Almeida, T. F. Silva, J. M. Assaf, *Catal. Today* **2020**, *344*, 124–128.

[11] W. W. Wang, P. P. Du, S. H. Zou, H. Y. He, R. X. Wang, Z. Jin, S. Shi, Y. Y. Huang, R. Si, Q. S. Song, C. J. Jia, C. H. Yan, *ACS Catal.* **2015**, *5*, 2088–2099.

[12] a) C. Papadopoulos, K. Kappis, J. Papavasiliou, J. Vakros, M. Kuśmierz, W. Gac, Y. Georgiou, Y. Deligiannakis, G. Avgouropoulos, *Catal. Today* **2020**, *355*, 647–653. b) J. Beckers, G. Rothenberg, *Dalt. Trans.* **2008**, 6573–6578.

[13] a) A. Uzunoglu, H. Zhang, S. Andreescu, L. A. Stanciu, *J. Mater. Sci.* **2015**, *50*, 3750–3762. b) Z. Lu, Z. Yang, B. He, C. Castleton, K. Hermansson, *Chem. Phys. Lett.* **2011**, *510*, 60–66.

[14] A. Chen, X. Yu, Y. Zhou, S. Miao, Y. Li, S. Kuld, J. Sehested, J. Liu, T. Aoki, S. Hong, M. F. Camellone, S. Fabris, J. Ning, C. Jin, C. Yang, A. Nefedov, C. Wöll, Y. Wang, W. Shen, *Nat. Catal.* **2019**, *2*, 334–341.

[15] S. D. Senanayake, J. A. Rodriguez, J. F. Weaver, *Acc. Chem. Res.* **2020**, *53*, 1488–1497.

[16] a) S. D. Senanayake, D. Stacchiola, J. A. Rodriguez, *Acc. Chem. Res.* **2013**, *46*, 1702–1711. b) F. Yang, J. Graciani, J. Evans, P. Liu, J. Hrbek, J. F. Sanz, J. A. Rodriguez, *J. Am. Chem. Soc.* **2011**, *133*, 3444–3451.

[17] a) Z. Zuo, P. J. Ramírez, S. D. Senanayake, P. Liu, J. A. Rodriguez, *J. Am. Chem. Soc.* **2016**, *138*, 13810–13813. b) Z. Liu, E. Huang, I. Orozco, W. Liao, R. M. Palomino, N. Rui, T. Duchoň, S. Nemšák, D. C. Grinter, M. Mahapatra, P. Liu, J. A. Rodriguez, S. D. Senanayake, *Science,* **2020**, *368*, 513–517.

[18] a) M. J. Muñoz-Batista, D. Rodriguez-Padron, A. R. Puente-Santiago, R. Luque, *ACS Sustain. Chem. Eng.* **2018**, *6*, 9530–9544. b) A. Danielis, M., Colussi, S., de Leitenburg, C., Soler, L., Llorca, J., Trovarelli, *Angew. Chemie - Int. Ed.* **2018**, *57*, 10212–10216. c) N. J. Divins, A. Braga, X. Vendrell, I. Serrano, X. Garcia, L. Soler, I. Lucentini, M. Danielis, A. Mussio, S. Colussi, I. J. Villar-Garcia, C. Escudero, A. Trovarelli, J. Llorca, *Nat. Commun.* **2022**, *13*, 5080.

[19] F. Sakina, J. M. Muñoz-Ocaña, A. Bouziane, M. Lopez-Haro, R. T. Baker, *Nanoscale Adv.* **2019**, *1*, 4772–4782.

[20] S. Zeng, Y. Wang, S. Ding, J. J.H.B. Sattler, E. Borodina, L. Zhang, B. M. Weckhuysen, J. Su, *Power Sources* **2014**, *256*, 301–311.

[21] G. Avgouropoulos, T. Ioannides, *Appl. Catal. B Environ.* **2006**, *67*, 1–11.

[22] a) M. Grioni, J. B. Goedkoop, R. Schoorl, F. M. F. de Groot, J. C. Fuggle, F. Schäfers, E. E. Koch, G. Rossi, J. M. Esteva, R. C. Karnatak, *Phys. Rev. B* **1989**, *39*, 1541–1545. b) M. Grioni, J. F. van Acker, M. T. Czyżyk, J. C. Fuggle, *Phys. Rev. B* **1992**, *45*, 3309-3318. c) F. Tavani, M. Fracchia, A. Tofoni, L. Braglia, A. Jouve, S. Morandi, M. Manzoli, P. Torelli, P. Ghigna, P. D'Angelo, *Phys. Chem. Chem. Phys.* **2021**, *23*, 26575–26584.

[23] a) L. A. J. Garvie, P. R. Buseck, *J. Phys. Chem. Solids* **1999**, *60*, 1943–1947. b) R. C. Karnatak, J. M. Esteva, H. Dexpert, M. Gasgnier, P. E. Caro, L. Albert, *Phys. Rev. B* **1987**, *36*, 1745–1749.

[24] B. T. Thole, G. van der Laan, J. C. Fuggle, G. A. Sawatzky, R. C. Karnatak, J. M. Esteva, *Phys. Rev. B* **1985**, *32*, 5107–5118.

[25] L. Braglia, F. Tavani, S. Mauri, R. Edla, D. Krizmancic, A. Tofoni, V. Colombo, P. D'Angelo, P. Torelli, *J. Phys. Chem. Lett.* **2021**, *12*, 9182–9187.

This article is protected by copyright. All rights reserved.

Author Manuscript

16136829, 2024, 42, Downloaded from https://onlinelibrary.wiley.com/doi/10.1002/smll.202403028 by CNR GROUP II Istituto di Scienza dell', Wiley Online Library on [06/03/2025]. See the Terms and Conditions (https://onlinelibrary.wiley.com/terms-and-conditions) on Wiley Online Library for rules of use; OA articles are governed by the applicable Creative Commons License

[26] C. Castán-Guerrero, D. Krizmancic, V. Bonanni, R. Edla, A. Deluisa, F. Salvador, G. Rossi, G. Panaccione, P. Torelli, *Rev. Sci. Instrum.* **2018**, *89*, 054101.

[27] A. Beck, M. Zabilskiy, M. A. Newton, O. Safonova, M. G. Willinger, J. A. van Bokhoven, *Nat. Catal.* **2021**, *4*, 488–497.

[28] a) M. Barreau, D. Chen, J. Zhang, V. Papaefthimiou, C. Petit, D. Salusso, E. Borfecchia, S. Turczyniak-Surdacka, K. Sobczak, S. Mauri, L. Braglia, P. Torelli, S. Zafeiratos, *Mater. Today Chem.* **2022**, *26*, 101011. b) S. Mauri, G. D'Olimpio, C. Ghica, L. Braglia, C. N. Kuo, M. C. Istrate, C. S. Lue, L. Ottaviano, T. Klimczuk, D. W. Boukhvalov, A. Politano, P. Torelli, *J. Phys. Chem. Lett.* **2023**, *14*, 1334–1342.

[29] a) J. Chrzan, M., Chlebda, D., Jodłowski, P., Salomon, E., Kołodziej, A., Gancarczyk, A., Sitarz, M., Łojewska, *Top. Catal.* **2019**, *62*, 403–412. b) S. T. Korhonen, M. A. Bañares, J. L. G. Fierro, A. O. I. Krause, *Catal. Today* **2007**, *126*, 235–247. c) S. Yin, Y., Liu, K., Gao, M., Zhang, L., Su, H., Zeng, *J. Mol. Catal. A Chem.* **2015**, *404–405*, 193–203. d) P. G. Lustemberg, M. V. Bosco, A. Bonivardi, H. F. Busnengo, M. V. Ganduglia-Pirovano, *J. Phys. Chem. C* **2015**, *119*, 21452–21464. e) P. J. Jodłowski, R. J. Jędrzejczyk, D. Chlebda, M. Gierada, J. Łojewska, *J. Catal.* **2017**, *350*, 1–12.

[30] M. M. Natile, G. Boccaletti, A. Glisenti, *Chem. Mater.* **2005**, *17*, 6272–6286.

[31] a) M. Mariño, F., Schönbrod, B., Moreno, M., Jobbágy, M., Baronetti, G., Laborde, *Catal. Today* **2008**, *133–135*, 735–742. b) C. G. Maclel, T. D. F. Silva, M. I. Hirooka, M. N. Belgacem, J. M. Assaf, *Fuel* **2012**, *97*, 245–252. c) Y. Zhou, K., Xu, R., Sun, X., Chen, H., Tian, Q., Shen, D., Li, *Catal. Letters* **2005**, *101*, 169–173. d) F. Giordano, A. Trovarelli, C. De Leitenburg, M. Giona, *J. Catal.* **2000**, *193*, 273–282.

[32] a)C. Li, K. Domen, K. Ichi Maruya, T. Onishi, *J. Catal.* **1990**, *125*, 445–455. b) C. Li, Y. Sakata, T. Arai, K. Domen, K. I. Maruya, T. Onishi, *J. Chem. Soc., Faraday Trans.* **1989**, *85*, 1451–1461. c) K. Yoshikawa, H. Sato, M. Kaneeda, J. N. Kondo, *J. CO2 Util.* **2014**, *8*, 34–38. d) C. Binet, M. Daturi, J. C. Lavalley, *Catal. Today* **1999**, *50*, 207–225. e) A. Badri, C. Binet, J.-C. Lavalley, *J. Chem. Soc., Faraday Trans.* **1996**, *92*, 4669–4673.

[33] a) G. Henkelman, B. P. Uberuaga, H. Jónsson, *J. Chem. Phys.* **2000**, *113*, 9901–9904. b) K. Bhola, J. J. Varghese, L. Dapeng, Y. Liu, S. H. Mushrif, *J. Phys. Chem. C* **2017**, *121*, 21343–21353.

[34] a) J. P. Perdew, K. Burke, M. Ernzerhof, *Phys. Rev. Lett.* **1996**, *77*, 3865–3868. b) S. Fabris, S. De Gironcoli, S. Baroni, G. Vicario, G. Balducci, *Phys. Rev. B - Condens. Matter Mater. Phys.* **2005**, *71*, 6–9. c) C. E. Ekuma, V. I. Anisimov, J. Moreno, M. Jarrell, *Eur. Phys. J. B* **2014**, *87*, 1–6. d) P. Giannozzi, S. Baroni, N. Bonini, M. Calandra, R. Car, C. Cavazzoni, D. Ceresoli, G. L. Chiarotti, M. Cococcioni, I. Dabo, A. Dal Corso, S. De Gironcoli, S. Fabris, G. Fratesi, R. Gebauer, U. Gerstmann, C. Gougoussis, A. Kokalj, M. Lazzeri, L. Martin-Samos, N. Marzari, F. Mauri, R. Mazzarello, S. Paolini, A. Pasquarello, L. Paulatto, C. Sbraccia, S. Scandolo, G. Sclauzero, A. P. Seitsonen, A. Smogunov, P. Umari, R. M. Wentzcovitch, *J. Phys. Condens. Matter* **2009**, *21*, 395502.

Entry for the Table of Contents

This article is protected by copyright. All rights reserved.

Author Manuscript

16136829, 2024, 42, Downloaded from https://onlinelibrary.wiley.com/doi/10.1002/smll.202403028 by CNR GROUP II Istituto di Scienza dell', Wiley Online Library on [06/03/2025]. See the Terms and Conditions (https://onlinelibrary.wiley.com/terms-and-conditions) on Wiley Online Library for rules of use; OA articles are governed by the applicable Creative Commons License

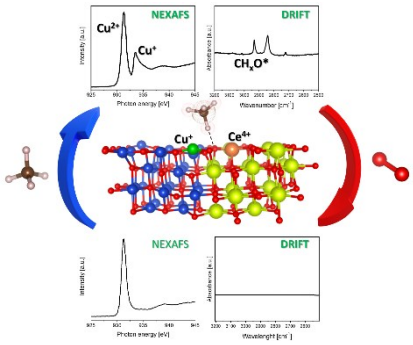

Methane activation on ball milled CeO_2/CuO catalysts has been studied with a combination of cutting-edge *operando* and *in-situ* spectroscopies. Thanks to *operando* NEXAFS we directly observed the formation of Cu^+ atoms. At the same time, activated methane species adsorbed on the surface of the milled CeO_2/CuO catalysts were observed through *in-situ* DRIFT. The adsorbates are desorbed from the surface after exposure to O_2, re-establishing the initial electronic structure at the catalyst surface. This reactivity is possible thanks to Cu^+/Ce^{4+} redox couples formed at the CeO_2-CuO interface as a consequence of the mechanochemical energy provided by ball milling.

Author Manuscript

WILEY VCH

This article is protected by copyright. All rights reserved.

16136829, 2024, 42, Downloaded from https://onlinelibrary.wiley.com/doi/10.1002/smll.202403028 by CNR GROUP II Istituto di Scienza dell', Wiley Online Library on [06/03/2025]. See the Terms and Conditions (https://onlinelibrary.wiley.com/terms-and-conditions) on Wiley Online Library for rules of use; OA articles are governed by the applicable Creative Commons License